IEEE Access
Multidisciplinary : Rapid Review : Open Access Journal

Received October 17, 2020, accepted November 6, 2020, date of publication November 10, 2020, date of current version December 9, 2020.

Digital Object Identifier 10.1109/ACCESS.2020.3037134

Voltage Regulation for Photovoltaics-Battery-Fuel Systems Using Adaptive Group Method of Data Handling Neural Networks (GMDH-NN)

SHAHAB S. BAND[1], ARDASHIR MOHAMMADZADEH[2], PETER CSIBA[3], AMIRHOSEIN MOSAVI[4,5], AND ANNAMARIA R. VARKONYI-KOCZY[3,6], (Fellow, IEEE)

[1]Future Technology Research Center, College of Future, National Yunlin University of Science and Technology, Yunlin 64002, Taiwan
[2]Department of Electrical Engineering, Faculty of Engineering, University of Bonab, Bonab, Iran
[3]Department of Informatics, J. Selye University, 94501 Komarno, Slovakia
[4]Environmental Quality, Atmospheric Science and Climate Change Research Group, Ton Duc Thang University, Ho Chi Minh City, Vietnam
[5]Faculty of Environment and Labour Safety, Ton Duc Thang University, Ho Chi Minh City, Vietnam
[6]Kalman Kando Faculty of Electrical Engineering, Obuda University, 1034 Budapest, Hungary

Corresponding authors: Amirhosein Mosavi (amirhosein.mosavi@tdtu.edu.vn) and Annamaria R. Varkonyi-Koczy (varkonyi-koczy@uni-obuda.hu)

This work was supported in part by the Project Support of Research and Development activities of the J. Selye University in the field of Digital Slovakia and creative industry of the Research and Innovation Operational Programme co-funded by the European Regional Development Fund (ITMS code) under Grant NFP313010T504, in part by the EFOP-3.6.2-16-2017-00016 project in the framework of the New Szechenyi Plan, in part by the European Union and co-financed by the European Social Fund, and in part by the Alexander von Humboldt Foundation.

ABSTRACT In this paper a new control system on basis of group method for data handling neural networks (GMDH-NNs) is designed for voltage and power regulation in the photovoltaic (PV)/Fuel/Battery systems. The dynamics of all subsystems are considered to be fully uncertain. The suggested GMDH-NN is learned using online tuning rules that are concluded through the robustness investigation. The challenging operation conditions such as variable unknown dynamics, unknown temperature and irradiation and suddenly changes in output load are taken into account and are handled by suggested control system. The superiority of the suggested method is shown by simulation in several scenarios and comparison with other techniques.

INDEX TERMS Adaptive control, GMDH, adaptive learning, energy management, PV panels, solar energy, machine learning.

I. INTRODUCTION

The importance of renewable energies such as PV panels is increasing day by day due to some attractive features such as abundance and clearity. However the efficiency of PV panels is significantly undesirable, because of high dependance on weather conditions. Then the PV panels need to be combined with storages systems such as batteries. Also fuel cells as the backup systems can be used to make a better energy balance. The control object is the output voltage to be regulated in a desired level in versus of variable load, temperature and irradiation.

Up to now, many management techniques have been presented. For instance, in [1], hybrid energy storage systems are investigated and various structure by combination of super-cap, battery, hydrogen and power-to-heat is studied. In [2], an management technique is presented by proposing a cost function including the decay cost of storage systems. In [3], a forecasting method on basis of Markov technique is presented to construct a power management planing considering various energy sources and cost of hydrogen consumption and electricity energy. In [4], the problem of energy consumption in peak hours is considered and a management system is designed for overall balancing. In [5], considering electrical vehicles in microgrids and the problem of fault event, a management method is proposed on basis of targeted search shuffled method. In [6], by genetic algorithm, an optimization problem is solved to minimize energy cost under step tariffs in a power system that includes PV and battery units. In [7], the effect of wind speed is investigated in a PV-battery-wind

The associate editor coordinating the review of this manuscript and approving it for publication was Jenny Mahoney.

system and a power management method is introduced to extract the maximum power form PV system. In [8], a voltage management method is presented to diminish the output voltage fluctuation by planing the charging and discharging of batter storage systems in peak hours. In [9], the problem of battery degradation is studied in the PV/battery systems by considering the effect of temperature.

In the most above studies, the dynamics are considered to be known and only an optimization problem is investigated. To cope with uncertainties, some fuzzy neural network (FNN) approach have been suggested. For example, in [10], a neural model is developed for PV panels and wind sources and it is shown that FNNs results in a good accuracy. A fractional-order fuzzy control approach is developed in [11], for both power and voltage management. In [12], the optimal utilization of batteries in hybrid systems is studied and the effectiveness of FNNs is shown. In [13], FNNs are used to increase the power extraction in PV systems and energy saving plan for battery is investigated. In [14], a FNN is learned by bat algorithm and it is applied for PV/battery system and the effect of shading conditions on power extraction is studied. In [15], similarly to [14], the FNNs are optimized to power and voltage regulation and the superiority of FNNs based control systems is shown. In [16], a predictive controller is developed using FNNs for power consumption management and the voltage regulation in daylight irradiation times is studied. In [17], deep discharging problem in PV/battery systems is studied using FNNs and it is shown that by the use of FNNs a better energy balance can be achieved. In [18], it is shown that the fuzzy based controllers improve the regulation accuracy about 12%. In [19], the problem of peak current in battery is considered and a FNN based controller is designed and it is shown that tuning of FNN by particle swarm optimization better reduces the peak current in contrast to traditional low-pass filters. In [20], a simple neural system is suggested to approximate the relationship between various energy generators and consumption units and on basis of the neural model an operation control system is designed using bus voltage.

The main shortcomings of the methods in the above-mentioned literature are summarized as follows. In the most of reviewed studies, simple FNNs are used and also the controller optimization is not adaptive and online. An optimization problem commonly is solved as off-line and the unpredictable conditions during process are neglected. Also the stability is not guaranteed. Motivated by above review, in this study a new neural controller is proposed. Unlike to the most papers, very difficult operation conditions are taken into account and robustness and stability are ensured. New GMDH approach with online and stable learning algorithm is suggested to deal with unknown dynamics of PV, battery and other units. In many studies and applications it is shown that GMDH based FNNs are more effective than conventional FNNs in nonlinear problems with high uncertainties such as: forecasting applications [21], modeling nonlinear systems [22], soil compaction analysis [23], electrical load

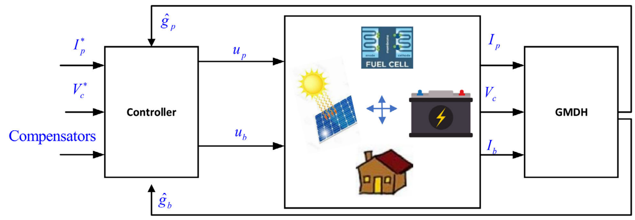

FIGURE 1. **A general view on control system: I_p/I_b and V_c are the PV/battery currents and output voltage respectively; u_p and u_b are control signals; $\hat{g}_p$ and $\hat{g}_p$ are outputs of suggested GMDH-NNs; I_p^* and V_c^* are reference signals.**

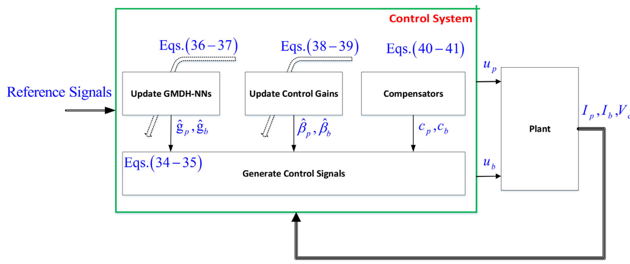

FIGURE 2. **A general view on control system.**

studies [24], feature extraction problems [25], classifier systems [26], and many others. The main advantages and contribution of current study are:

- A new approach on criteria of GMDH neural networks is presented
- Adaptive rules are obtained for online learning of GMDH-NNs.
- Unlike to the other methods, in addition to uncertain conditions such as time-varying temperature and irradiation, the dynamics are also considered to be unknown. Furthermore, abruptly changes in output load is considered to be external perturbation.
- New adaptive compensators guarantee the robustness.

In the remaining, the problem is formulated in Section II, the structure of GMDH-NN is explained in Section III, the main results are provided in Section IV, the simulations results are presented in Section V and finally the conclusions are given in Section VI.

II. PROBLEM FORMULATION

A. GENERAL VIEW

The block diagram of the under control plant is shown in Fig. 1. As it is observed, a GMDH-NN is employed to deal with uncertain dynamics of units. The controllers are designed on basis of GMDH model (see Fig. 2). The impacts of variable irradiation, temperature and estimation error are handled by compensators such that the robustness to be ensured. GMDH-NN is online learned by tuning laws that arise from stability study. It should be noted that there is no data set for learning of GMDH-NN. The input/output data set is online measured at each sample time.

TABLE 1. Parameter description of FC, see equation (1).

Parameter	Description	Unit
R	Constant of universal gas	J/mol K
T	Stack temperature	kelvin
F	Faraday's constant	C/mol
E_0	Voltage of free energy	volt
r	Stack internal resistance of	Ω
N_0	Number of cells in stack	-
I_{IC}	Current of FC	A
ρ_{H_2}	Hydrogen Partial pressures	atm
ρ_{H_2O}	Water Partial pressures	atm
ρ_{O_2}	Oxygen Partial pressures	atm

Remark 1: The main topic of this study is to present a control system for voltage and power regulation not a maximum power point tracking algorithm. Please note that, as shown in the general control block diagram (Fig. 2), it is assumed that the optimal current of PV is known. The main objective of this study is to design an adaptive control system such that a robust regulation performance to be achieved in versus of unknown mathematical dynamics, abrupt changes in output load and variation of temperature and irradiation.

B. FUEL UNIT

The fuel cells as the backup systems are used to improve the reliability of the system. The fuel cells help to full charge of battery storage systems. The FC unit is described as equations (1-6):

$$V_{FC} = N_0\left(\ln\left[\rho_{H_2}\cdot\rho_{O_2}^{0.5}/\rho_{H_2O}\right]\cdot\frac{TR}{2F}+E_0\right)-rI_{FC} \quad (1)$$

$$q_{H_2} = 2I_{FC}K_r/\left[\left(s\tau_f+1\right)U_{opt}\right] \quad (2)$$

$$q_{O_2^{in}} = q_{H_2^{in}}/r_{HO} \quad (3)$$

$$\rho_{H_2} = \left[-2K_rI_{FC}+q_{H_2^{in}}\right]/\left[k_{H_2}\left(s\tau_{H_2}+1\right)\right] \quad (4)$$

$$\rho_{O_2} = \left[-K_rI_{FC}+q_{O_2^{in}}\right]/\left[k_{O_2}\left(s\tau_{O_2}+1\right)\right] \quad (5)$$

$$\rho_{H_2O} = \left[2K_rI_{FC}\right]/\left[k_{H_2O}\left(s\tau_{H_2O}+1\right)\right] \quad (6)$$

where, the parameter are defined and described in Tables 1- 2.

C. CONVERTERS

The Boost convertors are used for applying control command on PV and battery/Fuel units to carry out an energy balance between energy generation and consumption. The Boost and Bidirectional Boost convertors as shown in Fig. 3, are considered the switching actuators. From Fig. 3, the circuits for all modes are depicted in Fig. 4. On basis of Fig. 4, the dynamics can be written as:

$$\begin{aligned}\dot{\chi}_1 &= \left(V_cu_p-\chi_2+V_p\left(\chi_1\right)\right)/L_p\\ \dot{\chi}_2 &= \frac{1}{C}\left(-\chi_1u_p+\chi_1-\chi_2/R+I_bu_b\right)\\ \dot{\chi}_3 &= \left(V_b\left(\chi_3\right)-\chi_2u_b\right)/L_b\end{aligned} \quad (7)$$

where, V_c and I_p/I_b are the load voltage and currents of PV/battery. L_p, L_b and C are the values of inductors and capacitor and R represents the output load. u_p, u_b are control signals. V_p and V_b are voltage of PV and battery. The variables χ_1, χ_2 and χ_3 are considered to be I_p, V_c and I_b, respectively.

TABLE 2. Parameter description of FC, see equations (2-6).

Parameter	Description	Unit
k_{H_2}	Valve molar index of hydrogen	kmol/s· atm
q_{H_2}	Hydrogen flow rate	mol/s
τ_{H_2}	Time constant of hydrogen	sec
k_{O_2}	Valve molar index of oxygen	kmol/s · atm
q_{O_2}	Oxygen flow rate	mol/s
τ_{O_2}	Time constant of oxygen	sec
k_{H_2O}	Valve molar index of water	kmol/s· atm
τ_{H_2O}	Time constant of water	sec
K_r	constant	kmol/s · A
τ_f	Time constant of fuel	sec
r_{HO}	Hydrogen to oxygen ratio	-
U_{opt}	Desired level of fuel employment	-

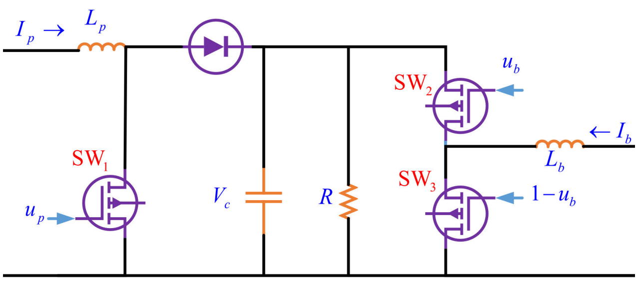

FIGURE 3. Boost and Bidirectional Boost convertors: I_p/I_b and V_c are the PV/battery currents and output voltage respectively; u_p and u_b are control signals; SW_1, SW_2 and SW_3 are switchers; L_p and L_b are the value of inductors and R represents the output load.

TABLE 3. Parameter definition of PV, see equation (8).

Parameter	Description
n	Cell numbers
$G\ (w/m^2)$	Solar radiation
$k_b\ (J/K)$	Boltzmann's constant
R_{sh} and $R_s\ (\Omega)$	Equivalent resistances
$E_g\ (ev)$	Band-Gap Energy
q	Electron charge
$T\ (°c)$	PV Temperature
A	Diode ideality constant
$i_{ph}\ (A)$	Currents generated by photo
$T_r\ (°c)$	Desired temperature
$i_r\ (A)$	Current of saturation

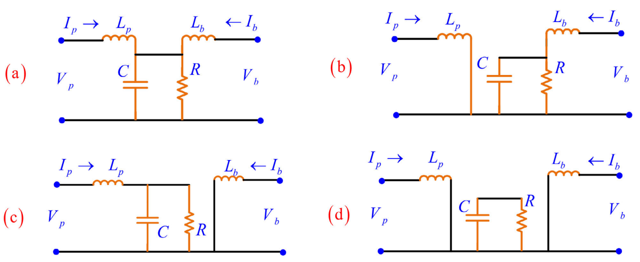

FIGURE 4. Four switching modes while the state of switchers SW_1/SW_2/SW_3 is: (a): open/close/open; (b): close/close/open; (c): open/open/close; (d): close/open/close. I_p and I_b are the currents of PV and battery; V_p and V_b are voltage of PV and battery; L_p, L_b and C are the values of inductors and capacitor and R represents the output load.

D. PV MODELING

On basis of single-diode modeling of PV panels [27], one has:

$$\begin{aligned} i_{ph} &= s\left(i_{sc} + k_i\left(T - T_r\right)\right) \\ I_p &= I_{phg}G - i_o \exp\left(-1 + q\left(V_p + I_pR_{sg}\right)/nTk_b\right) \\ &\quad - \frac{1}{R_{shg}}\left(V_p + I_pR_{sg}\right) \\ i_0 &= \exp\left[E_g q \frac{\left(\frac{1}{T_r+273} - \frac{1}{T+273}\right)}{k_bA}\right]\left(T + 273/T_r + 273\right)^3 i_r \end{aligned} \tag{8}$$

where, definition of parameters are given in Table 3. The trajectory of power of PV as a function of its current is shown in Fig. 5. It is seen that at one current, the maximum power can be obtained. The frequency switching should be adjusted such that the current of PV to regulated at its optimal level.

E. BATTERY MODELING

The battery dynamics can be described by equation (9-12) [27]:

$$E\left(t\right) = -\int \beta V_{boc}I_b + W_{Loss}dt \tag{9}$$

$$V_b = -r_bI_b + V_{boc} \tag{10}$$

$$SoC\left(t\right) = E\left(t\right)/E_{\mathrm{Max}} \tag{11}$$

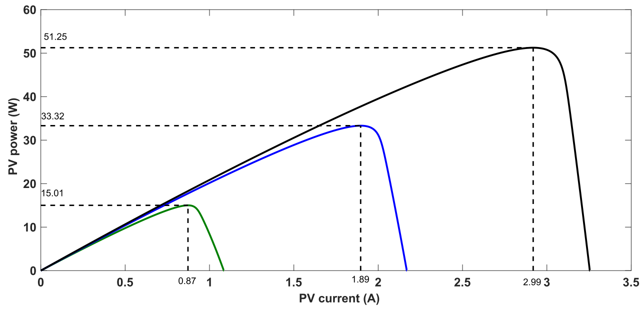

FIGURE 5. The power trajectories of the under control PV panel with respect to the current.

TABLE 4. Parameter description of battery system, see equation (9).

Parameter	Description
$r_b\ (\Omega)$	Internal resistance
$W_{Loss}\ (w)$	Power losses
β_1 and β_2	Charge/discharge rate
$V_{boc}\ (v)$	Open circuit voltage
$E_{\mathrm{Max}}\ (J)$	Maximum charging level

where,

$$\beta = \begin{cases} \beta_1 & I_b \geq 0 \\ \beta_2 & I_b < 0 \end{cases} \tag{12}$$

where, E represents the charging level and V_b and I_b are the voltage and current of battery. The other parameters are given in Table 4.

III. UNCERTAINTY APPROXIMATION BY GMDH-NN

The dynamics of all units reconsidered to be unknown and time-varying. As depicted in Fig. 6, GMDH-NNs are employed to estimate the dynamics. The details are explained in below.

1) The inputs of GMDH-NNs are χ_1, χ_2 and χ_3. Then considering Ivakhnenko second order polynomials, for 3 input variables, there will be two neurons with five sub-neurons.

2) For the first and second neurons in the hidden layer one has:

$$\begin{aligned} x_{11} &= \chi_1 \\ x_{12} &= \chi_2 \\ x_{13} &= \chi_1\chi_1 \\ x_{14} &= \chi_1^2 \\ x_{15} &= \chi_2^2 \end{aligned} \tag{13}$$

$$\begin{aligned} x_{21} &= \chi_2 \\ x_{22} &= \chi_3 \\ x_{23} &= \chi_2\chi_3 \\ x_{24} &= \chi_2^2 \\ x_{25} &= \chi_3^2 \end{aligned} \tag{14}$$

3) The inputs of output neuron are obtained as:

$$o_{h1} = f\left(w_{i2}^T x_1\right) \tag{15}$$

$$o_{h2} = f\left(w_{i2}^T x_2\right) \tag{16}$$

where, o_{h1} and o_{h2} represent the outputs of hidden neurons and:

$$w_{i1} = \left[w^i_{11}, w^i_{12}, \ldots, w^i_{15}\right]^T \tag{17}$$
$$w_{i2} = \left[w^i_{21}, w^i_{22}, \ldots, w^i_{25}\right]^T \tag{18}$$
$$x_1 = [x_{11}, x_{12}, \ldots, x_{15}]^T \tag{19}$$
$$x_2 = [x_{21}, x_{22}, \ldots, x_{25}]^T \tag{20}$$
$$f(\chi) = \frac{1-\exp(-\chi)}{1+\exp(-\chi)} \tag{21}$$

4) For the output neuron, one has:

$$\hat{g}_i = w_{i3}^T \phi_i \tag{22}$$

where similarly to (17-18), w_{i3} is the vector of parameters in output layer and:

$$\phi_i = \left[o^i_{h1}, o^i_{h2}, o^i_{h1}o^i_{h2}, \left[o^i_{h1}\right]^2, \left[o^i_{h2}\right]^2\right]^T \tag{23}$$

Considering Taylor expansion, $\hat{g}_i$ in (22) can be written as:

$$\hat{g}_i \approx \theta_i^T \varphi_i \tag{24}$$
$$\theta_i^T = \begin{bmatrix} w_{i1}^T & w_{i2}^T & w_{i3}^T \end{bmatrix} \tag{25}$$
$$\varphi_i^T = \begin{bmatrix} \frac{\partial \hat{g}_i}{\partial w_{i1}} & \frac{\partial \hat{g}_i}{\partial w_{i2}} & \frac{\partial \hat{g}_i}{\partial w_{i3}} \end{bmatrix} \tag{26}$$

From (26), for $\frac{\partial \hat{g}_i}{\partial w_{i3}}$, one has:

$$\frac{\partial \hat{g}_i}{\partial w_{i3}} = \left[o^i_{h1}, o^i_{h2}, o^i_{h1}o^i_{h2}, \left[o^i_{h1}\right]^2, \left[o^i_{h2}\right]^2\right] \tag{27}$$

For $\frac{\partial \hat{g}_i}{\partial w_{i1}}$, one has:

$$\frac{\partial \hat{g}_i}{\partial w_{i1}} = \delta_{i1} f'\left(w_{i1}^T x_1\right) x_1 \tag{28}$$

where,

$$f'\left(w_{i1}^T x_1\right) = \frac{2\exp\left(-w_{i1}^T x_1\right)}{\left(1+\exp\left(-w_{i1}^T x_1\right)\right)^2} \tag{29}$$
$$\delta_{i1} = w^i_{31} + w^i_{32} o^i_{h2} + 2w^i_{34} o^i_{h1} \tag{30}$$

Similarly to (28), $\frac{\partial \hat{g}_i}{\partial w_{i2}}$ can be obtained as:

$$\frac{\partial \hat{g}_i}{\partial w_{i2}} = \delta_{i2} f'\left(w_{i2}^T x_2\right) x_2 \tag{31}$$

where,

$$f'\left(w_{i2}^T x_2\right) = \frac{2\exp\left(-w_{i2}^T x_2\right)}{\left(1+\exp\left(-w_{i2}^T x_2\right)\right)^2} \tag{32}$$
$$\delta_{i2} = w^i_{32} + w^i_{32} o^i_{h1} + 2w^i_{35} o^i_{h2} \tag{33}$$

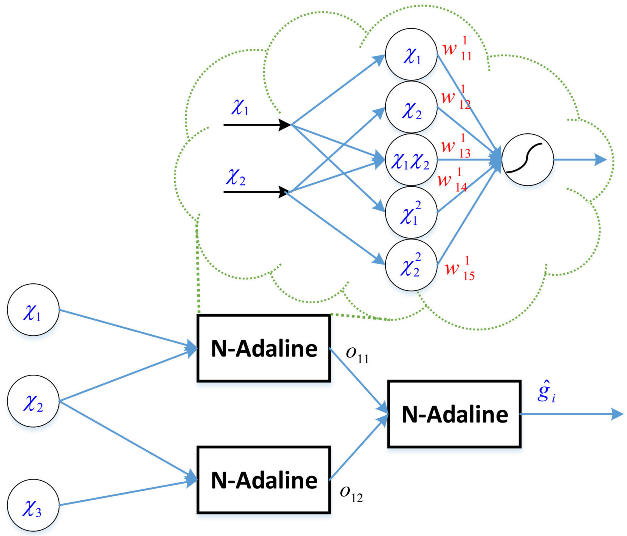

FIGURE 6. The structure of suggested estimator: $\chi_1 = I_p$, $\chi_2 = V_c$ and $\chi_3 = I_b$ are the input signals, w^1_{1j}, $j = 1, \ldots, 5$ are the tunable parameters and $\hat{g}_i$ is the output of the suggested GMDH-NN.

IV. MAIN RESULTS

The main results and outcomes are given in the following theorem.

Theorem 1: If the adaptation rules, controllers and compensators are considered as (34-41), then the asymptotic stability is ensured.

$$u_p = \left(-\iota_p e_p - \hat{g}_p + c_p\right)/\hat{\beta}_p \tag{34}$$
$$u_b = \left(-\iota_p e_b - \hat{g}_b + c_b\right)/\hat{\beta}_b \tag{35}$$
$$\dot{\hat{\theta}}_b = \lambda \tilde{V}_c \varphi_b \tag{36}$$
$$\dot{\hat{\theta}}_p = \lambda \tilde{I}_p \varphi_p \tag{37}$$
$$\dot{\hat{\beta}}_p = \lambda \tilde{I}_p V_c u_p \tag{38}$$
$$\dot{\hat{\beta}}_b = \lambda \tilde{V}_c I_b u_b \tag{39}$$
$$c_p = -\bar{\Pi}_p e_p \left|\tilde{I}_p\right| / \left(\left|e_p\right| + \delta\right) \tag{40}$$
$$c_b = -\bar{\Pi}_b e_b \left|\tilde{V}_c\right| / \left(\left|e_b\right| + \delta\right) \tag{41}$$

where, λ, ι_b, ι_p, $\bar{\Pi}_b$ and $\bar{\Pi}_p$ are constant, δ, c_b and c_p are compensators, e_p and e_b are tracking errors.

Proof: From (7), the output dynamics can be rewritten as:

$$\dot{I}_p = \left(-V_c + V_p\left(I_p\right)\right)/L_p + \frac{V_c}{L_p} u_p$$
$$\dot{V}_c = \left(I_p/C - I_p u_p/C - V_c/CR\right) + \frac{I_b}{C} u_b \tag{42}$$

To design controllers u_p and u_b, the estimated dynamics are considered as:

$$\dot{\hat{I}}_p = \hat{g}_p + \hat{\beta}_p V_c u_p$$
$$\dot{\hat{V}}_c = \hat{g}_b + \hat{\beta}_b I_b u_b \tag{43}$$

where $\hat{\beta}_p$ and $\hat{\beta}_b$ are estimations of $1/L_p$ and $1/C$. $\hat{g}_p$ and $\hat{g}_b$ are the GMDH-NN. The dynamics of $\tilde{I}_p = I_p - \hat{I}_p$ and $\tilde{V}_c = V_c - \hat{V}_c$ are:

$$\begin{aligned}\dot{\tilde{I}}_p &= \left(-V_c + V_p\left(I_p\right)\right)/L_p - \hat{g}_p \\ &\quad + \left(\frac{1}{L_p} - \hat{\beta}_p\right) V_c u_p \\ \dot{\tilde{V}}_c &= \left(I_p/C - I_p u_p/C - V_c/CR\right) - \hat{g}_b \\ &\quad + \left(\frac{1}{C} - \hat{\beta}_b\right) I_b u_b \end{aligned} \tag{44}$$

From (44), $\dot{\tilde{I}}_p$ and $\dot{\tilde{V}}_c$ are written as:

$$\begin{aligned}\dot{\tilde{I}}_p &= \left[\left(-V_c + V_p\left(I_p\right)\right)/L_p - \hat{g}_p^*\right] + \hat{g}_p^* - \hat{g}_p \\ &\quad + \left(\hat{\beta}_p^* - \hat{\beta}_p\right) V_c u_p + \left(\frac{1}{L_p} - \hat{\beta}_p^*\right) V_c u_p \\ \dot{\tilde{V}}_c &= \left[\left(I_p/C - I_p u_p/C - V_c/CR\right) - \hat{g}_b^*\right] + \hat{g}_b^* - \hat{g}_b \\ &\quad + \left(\hat{\beta}_b^* - \hat{\beta}_b\right) I_b u_b + \left(\frac{1}{C} - \hat{\beta}_b^*\right) I_b u_b \end{aligned} \tag{45}$$

where, $\hat{g}_b^*$ and $\hat{g}_p^*$ are optimal GMDH-NN. From (45), the approximation errors E_p and E_b are considered as:

$$\begin{aligned}E_p &= \left[\left(-V_c + V_p\left(I_p\right)\right)/L_p - \hat{g}_p^*\right] + \left(\frac{1}{L_p} - \hat{\beta}_p^*\right) V_c u_p \\ E_b &= \left(\chi_1/C - \chi_1 u_p/C - \chi_2/CR\right) - \hat{g}_2^*\left(\chi, \theta_b^*\right) \\ &\quad + \left(\frac{1}{C} - \hat{\delta}_2^*\right) I_b u_b \end{aligned} \tag{46}$$

From equations (45)-(46), one has:

$$\begin{aligned}\dot{\tilde{I}}_p &= E_p + \tilde{\theta}_p^T \varphi_p + \tilde{\beta}_p V_c u_p \\ \dot{\tilde{V}}_c &= E_b + \tilde{\theta}_b^T \varphi_2 + \tilde{\beta}_b I_b u_b \end{aligned} \tag{47}$$

where,

$$\begin{aligned}\tilde{\theta}_p &= \hat{\theta}_p^* - \hat{\theta}_p \\ \tilde{\theta}_b &= \hat{\theta}_b^* - \hat{\theta}_b \\ \tilde{\beta}_p &= \hat{\beta}_p^* - \hat{\beta}_p \\ \tilde{\beta}_b &= \hat{\beta}_b^* - \hat{\beta}_b \end{aligned} \tag{48}$$

Substituting the signals u_p and u_b from equations (34-35) one has:

$$\dot{e}_p = -\iota_p e_p + c_p \tag{49}$$

$$\dot{e}_b = -\iota_b e_b + c_b \tag{50}$$

Now, to prove stability, Lyapunov function is defined as:

$$\begin{aligned}V &= \frac{1}{2}\tilde{I}_p^2 + \frac{1}{2}\tilde{V}_c^2 + \frac{1}{2}e_p^2 + \frac{1}{2}e_b^2 \\ &\quad \times \frac{1}{2\lambda}\tilde{\beta}_p^2 + \frac{1}{2\lambda}\tilde{\beta}_b^2 + \frac{1}{2\lambda}\tilde{\theta}_p^T\tilde{\theta}_p + \frac{1}{2\lambda}\tilde{\theta}_b^T\tilde{\theta}_b \end{aligned} \tag{51}$$

From (51), $\dot{V}$ is concluded that:

$$\begin{aligned}\dot{V} &= \dot{\tilde{I}}_p\tilde{I}_p + \dot{\tilde{V}}_c\tilde{V}_c + \dot{e}_p e_p + \dot{e}_b e_b \\ &\quad - \frac{1}{\lambda}\tilde{\beta}_p\dot{\hat{\beta}}_p - \frac{1}{\lambda}\tilde{\beta}_b\dot{\hat{\beta}}_b - \frac{1}{\lambda}\tilde{\theta}_p^T\dot{\hat{\theta}}_p - \frac{1}{\lambda}\tilde{\theta}_b^T\dot{\hat{\theta}}_b \end{aligned} \tag{52}$$

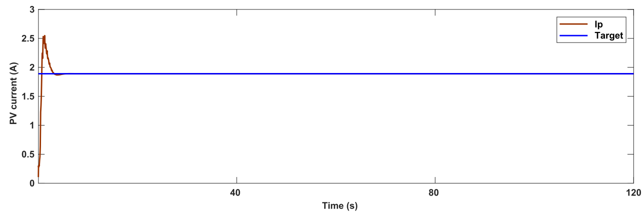

FIGURE 7. Scenario 1: Trajectory of I_p.

Then, $\dot{V}$ yields as:

$$\begin{aligned}\dot{V} &= \tilde{I}_p\left(\Pi_p + \tilde{\theta}_p^T\varphi_p + \tilde{\beta}_p V_c u_p\right) + \tilde{V}_c\left(\Pi_b + \tilde{\theta}_b^T\varphi_2 + \tilde{\beta}_b I_b u_b\right) \\ &\quad + e_p\left(-\iota_p e_p + c_p\right) + e_b\left(-\iota_b e_b + c_b\right) \\ &\quad - \frac{1}{\lambda}\tilde{\beta}_p\dot{\hat{\beta}}_p - \frac{1}{\lambda}\tilde{\beta}_b\dot{\hat{\beta}}_b - \frac{1}{\lambda}\tilde{\theta}_p^T\dot{\hat{\theta}}_p - \frac{1}{\lambda}\tilde{\theta}_b^T\dot{\hat{\theta}}_b \end{aligned} \tag{53}$$

From (53), $\dot{V}$ is written:

$$\begin{aligned}\dot{V} &= -\iota_p e_p^2 + c_p e_p - \iota_b e_b^2 + c_b e_b \\ &\quad + \tilde{\theta}_p^T\left(\tilde{I}_p\varphi_p - \frac{1}{\lambda}\dot{\hat{\theta}}_p\right) + \tilde{\theta}_b^T\left(\tilde{V}_c\varphi_b - \frac{1}{\lambda}\dot{\hat{\theta}}_b\right) \\ &\quad + \tilde{\beta}_p\left(\tilde{I}_p V_c u_p - \frac{1}{\lambda}\dot{\hat{\beta}}_p\right) + \tilde{\beta}_b\left(\tilde{V}_c I_b u_b - \frac{1}{\lambda}\dot{\hat{\beta}}_b\right) \\ &\quad + \Pi_p\tilde{I}_p + \Pi_b\tilde{V}_c \end{aligned} \tag{54}$$

Considering tuning rules $\dot{\hat{\theta}}_b = \lambda\tilde{V}_c\varphi_b$, $\dot{\hat{\theta}}_p = \lambda\tilde{I}_{pc}\varphi_p$, $\dot{\hat{\beta}}_b = \lambda\tilde{V}_c I_b u_b$ and $\dot{\hat{\beta}}_p = \lambda\tilde{I}_p V_c u_p$ from (36-39), $\dot{V}$ is written as:

$$\dot{V} = -\iota_b e_b^2 - \iota_p e_p^2 + c_p e_p + c_b e_b + \Pi_p\tilde{I}_p + \Pi_b\tilde{V}_c \tag{55}$$

Then one has:

$$\begin{aligned}\dot{V} &\leq -\iota_b e_b^2 - \iota_p e_p^2 \\ &\quad + \left[\left|\Pi_p\right|\left|\tilde{I}_p\right| + c_p e_p\right] + \left[c_b e_b + \left|\Pi_b\right|\left|\tilde{V}_c\right|\right] \end{aligned} \tag{56}$$

Considering compensators c_p and c_b from (40-41), results in:

$$\begin{aligned}\dot{V} &\leq -\iota_b e_b^2 - \iota_p e_p^2 + \left|\Pi_b\right|\left|\tilde{I}_p\right| - \bar{\Pi}_b\left|\tilde{I}_p\right| e_p^2/\left(\left|e_p\right| + \delta\right) \\ &\quad + \left|\Pi_p\right|\left|\tilde{I}_b\right| - \bar{\Pi}_p\left|\tilde{I}_b\right| e_b^2/\left(\left|e_b\right| + \delta\right) \end{aligned} \tag{57}$$

From (57) it is concluded that $\dot{V} \leq 0$ and considering Barbalat's Lemma the proof is completed. □

Remark 2: It should be noted that, to guarantee the stability against dynamics perturbations such as variation of irradiation, output load and temperature, it is assumed that the upper bounds of perturbations are unknown. By the use of these upper bounds, the suggested compensators are designed. Furthermore, it is assumed that there is no restricts on control signals and the generated control signals can be handled by the actuator. Then, by considering the upper bounds of perturbations, and assuming no limitation on control signals, the range of variation of irradiation, temperature and output load can be determined. For our future studies, the upper bounds of perturbations are assumed to be unknown and some adaptation laws are derived.

TABLE 5. Simulation parameters.

Parameter	value	Parameter	value
L_p	3 (mH)	L_b	20 (mH)
q	1.5e-19	n	36
P_b	65 (w)	i_{sc}	4.45 (A)
C	600 (μf)	r_p	40 $(m\Omega)$
r_b	80 $(m\Omega)$	k_b	1.481e-23
T_r	$(^{\circ}C)$	k_i	1.5 (A/k)
A	1.2	V_{boc}	8 (v)
β_1	0.97	β_2	1.13
i_r	2.93e-8 (A)	E_g	1.22 (ev)
P_b	22 (w)	W_{Loss}	22 (w)

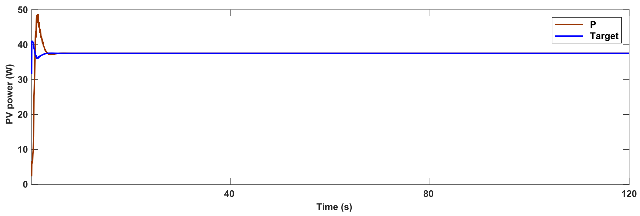

FIGURE 8. Scenario 1: Trajectory of P.

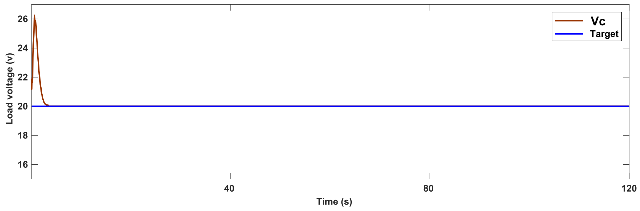

FIGURE 9. Scenario 1: Trajectory of V_c.

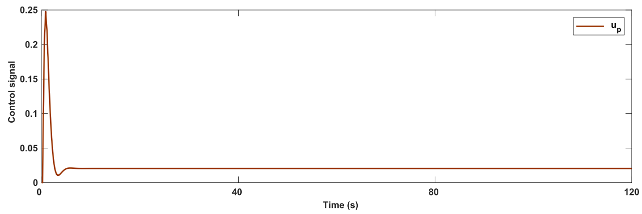

FIGURE 10. Scenario 1: Trajectory of u_p.

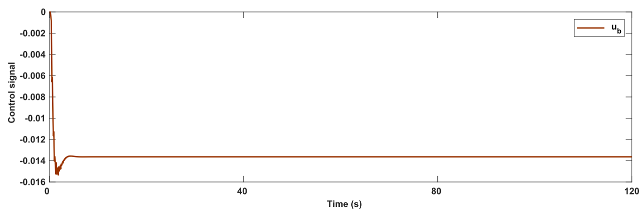

FIGURE 11. Scenario 1: Trajectory of u_b.

TABLE 6. MSE Comparison for different control methods.

Method	Signal V_c	Signal I_p
LQR [30]	137.9198	2.2237
PID [28]	178.134	2.8021
F-FLC [11]	8.1254	1.1427
PBC [29]	12.1340	0.9149
SMC [31]	9.4587	0.5761
Proposed Method	0.9071	0.3071

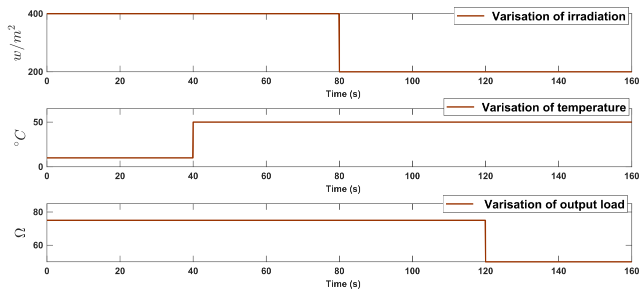

FIGURE 12. Scenario 2: Variation of irradiation, output load and temperature.

V. SIMULATION STUDIES

In several faulty condition, the regulation performance is examined. The values simulation parameters are provided in Table 5.

A. SCENARIO 1

For the first experiment, the normal condition is taken into account as follows. The irradiation, temperature and output load are considered to be fixed. The tracking performance of I_p, P, V_c are shown in Figs. 7- 9. The controller outputs u_p and u_b are shown in Figs. 10- 11. Figs. 7- 9 exhibit a good and favorable reference tracking response. Also one can see the good and implementable controller trajectories with no chattering in Figs. 10- 11.

B. SCENARIO 2

For 2-th scenario, a difficult condition is considered. Variation of irradiation, output load and temperature are depicted in Fig. 12. As shown in Fig. 12, the temperature is not constant but it is continuously changed from $T = 10$ to $T = 50\,^{\circ}C$, also output load is abruptly changed from 75 into 25 (Ω). Furthermore, irradiation level is suddenly changed from 400 into 200 (w/m^2). The tracking performance of I_p, P, V_c are shown in Figs. 13- 14. The controller outputs u_p and u_b are shown in Figs. 16- 17. From trajectories, a very good robustness is seen in the presence of variable temperature, irradiation and output load. The output voltage has been

TABLE 7. Comparison of tracking performance for different control methods in time range $t \in [0, 40]$.

t	Method	Overshoot	Undershoot	Settling time	Steady state error
I_p	LQR [30]	19.5358	0	-	0.1175
	PID [28]	27.35	19.58	34.85	0.0101
	F-FLC [11]	26.48	9.52	20.67	0.0014
	PBC [29]	21.75	6.88	39.79	0.0410
	SMC [31]	25.6395	8.98	26.83	0.0153
	Proposed Method	24.08	0	3.45	0.0001
V_c	LQR [30]	50.45	0	37.01	0.1649
	PID [28]	63.45	38.04	-	0.6816
	F-FLC [11]	15.40	4	12.30	0.0123
	PBC [29]	18.10	3.75	29.67	0.1887
	SMC [31]	21.11	3.60	20.30	0.0367
	Proposed Method	31.55	0	2.92	0.0087

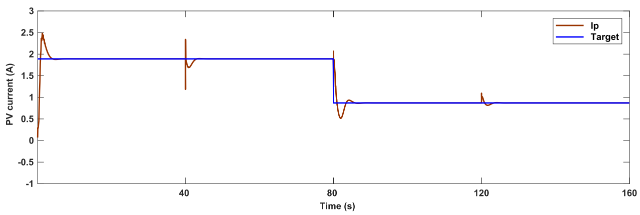

FIGURE 13. Scenario 2: Trajectory of I_p.

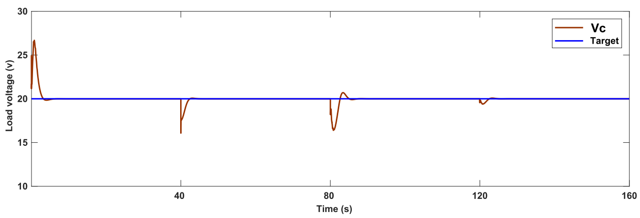

FIGURE 14. Scenario 2: Trajectory of V_c.

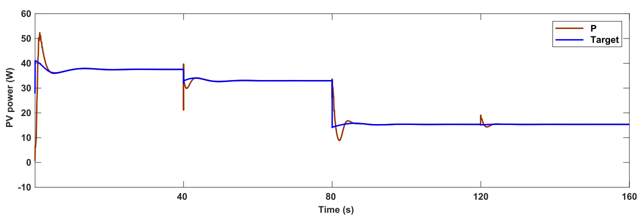

FIGURE 15. Scenario 2: Trajectory of P.

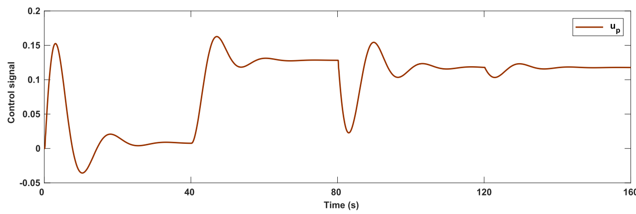

FIGURE 16. Scenario 2: Trajectory of u_p.

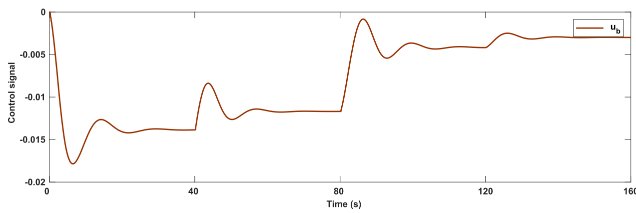

FIGURE 17. Scenario 2: Trajectory of u_b.

kept in favorable level and also the power well follows up the optimal operation point. It can be observed that, after disturbance occurring at times $t = 40s$, $t = 80s$ and $t = 120s$ the output voltage is converged to desired level 20 V in less than 20s. Furthermore, the shapes of control signals u_p and u_b are smooth with no fluctuation. Figs. 13- 14, demonstrate that the suggested controller exhibits a good robust performance against changes of output load, irradiation and temperature.

C. COMPARISON

In this experiment, a comparison with classic regulators is provided, such as: PID [28], passivity approach (PBC) [29], LQR [30], fractional-order fuzzy logic controller (F-FLC) [11], and sliding mode controller (SMC) [31]. The simulation conditions as given in the second scenario are considered to be same for all controllers. Table 6 exhibits the superiority of the suggested method. From Table 6, it can be realized that MSE (mean square error) values for suggested method is significantly less than the other approaches. It should be reminded that, this favorable performance is achieved, while unlike to the compared methods, the dynamics of PV panel and all other units are considered to be unknown. In other words, the mathematical model of these units are not used in the control designing process. The unknown dynamics are online estimated by the suggested GMDH-NNs. For better comparison, the trajectories of I_p and V_c for different above described controllers are depicted in Fig. 18. It is seen that the settling time for the suggested controller is significantly small than other methods. Also the value of steady state error for the suggested method is remarkable less than other techniques. The numerical compression in terms of overshoot, undershoot, steady state error and settling time are given Tables 7- 8.

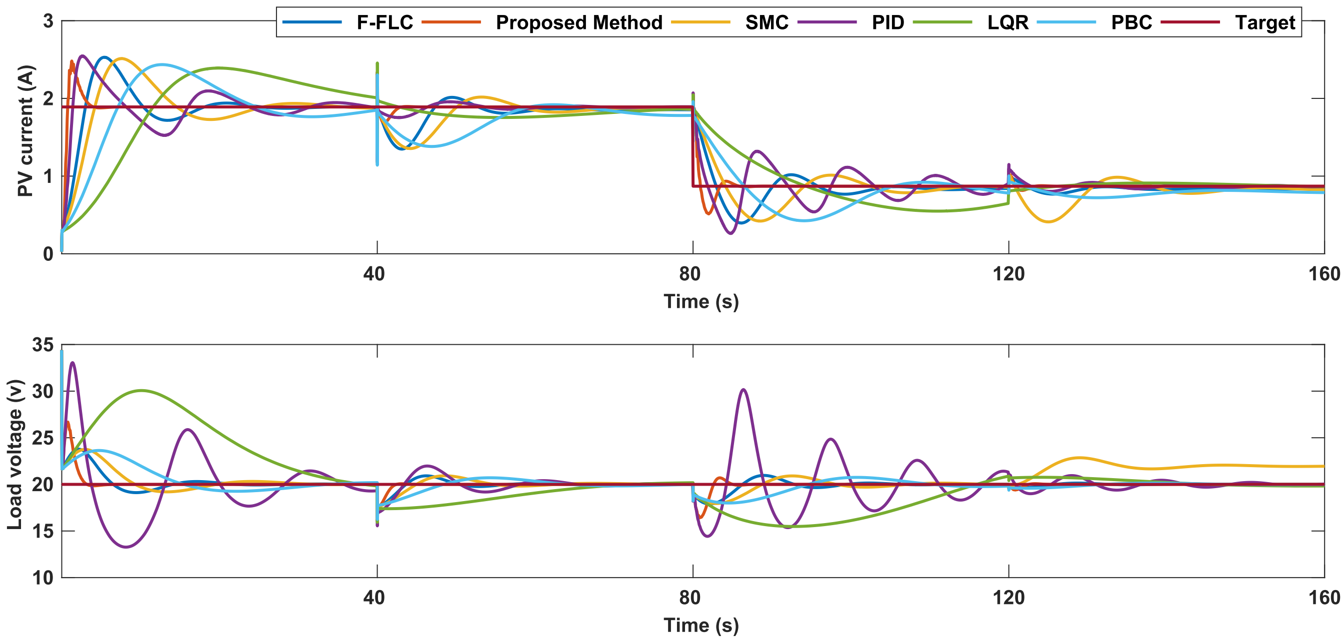

FIGURE 18. Trajectories of I_p and V_c for different control systems.

TABLE 8. Comparison of tracking performance for different control methods in time range $t \in [40, 80]$.

t	Method	Overshoot	Undershoot	Settling time	Steady state error
I_p	LQR [30]	19.5358	0	-	0.1175
	PID [28]	3.17	6.88	3.17	0.0101
	F-FLC [11]	6.35	28.04	18.70	0.0021
	PBC [29]	0.53	26.48	34.73	0.06
	SMC [31]	28.6395	18.98	32.62	0.0023
	Proposed Method	0	11.64	3.79	0
V_c	LQR [30]	0	15	29.25	0.1771
	PID [28]	9.6	19.6	22.1 0.0058	
	F-FLC [11]	6.51	17.50	19.5	0.0149
	PBC [29]	14.12	20.12	23.70	0.0062
	SMC [31]	6.45	20.01	15.16	0.0366
	Proposed Method	0	7.5	3.1	0.0003

Remark 3: The sample time in the simulations is 0.001s and it is equal for both controllers and GMDH-NNs. In other words, at each sample time the computations for updating the parameters of GMDH-NNs are done and then the control signals are generated (see Fig. 2).

Remark 4: The value of MSEs show the accuracy of the suggested control system. The smaller MSEs represent the higher accuracy. When the mean square of output voltage error is decreased the output voltage is converged to the desired voltage level. Also, the decreasing of mean square of PV current error indicates the approaching of the PV working point into optimal one.

Remark 5: It should be noted that, the parameters of suggested GMDH-NNs are tuned by the adaptation laws that are extracted form robustness and stability investigation. Then, by convergence the estimation errors into zero, the tracking errors are also reached to zero. As it can be seen form Figs. 7, 9, 13, 14, the trajectories of outputs are reached to their reference signals less than 20s.

VI. CONCLUSION

In this paper the problem of voltage and power adjustment in PV/Battery/Fuel systems is studied. A new approach is presented using GMDH-NN. GMDH-NNs are used to estimate uncertainties in dynamics of subsystems. New rules are extracted from robustness investigation for online learning of GMDH-NNs. The stability is ensured by compensators. Simulation results show the superiority of suggested approach against uncertain irradiation and temperature, unknown time-varying dynamics and output load. Also, a comparison with some classic regulators such as LQR, SMC and passivity based controllers, further clarifies the effectiveness of the suggested controller. One of the drawbacks of this study is that the desirable level of current of PV (reference signal) is considered to be known. For the future studies, a maximum power point tracking algorithm can be added to the suggested control scheme to determine the optimal current level of PV.

REFERENCES

[1] X. Lin and Y. Lei, "Coordinated control strategies for SMES-battery hybrid energy storage systems," *IEEE Access*, vol. 5, pp. 23452–23465, 2017.

[2] F. Nadeem, S. M. S. Hussain, P. K. Tiwari, A. K. Goswami, and T. S. Ustun, "Comparative review of energy storage systems, their roles, and impacts on future power systems," *IEEE Access*, vol. 7, pp. 4555–4585, 2019.

[3] Y. Wang, X. Li, L. Wang, and Z. Sun, "Multiple-grained velocity prediction and energy management strategy for hybrid propulsion systems," *J. Energy Storage*, vol. 26, Dec. 2019, Art. no. 100950.

[4] N. Javaid, S. Cheema, M. Akbar, N. Alrajeh, M. S. Alabed, and N. Guizani, "Balanced energy consumption based adaptive routing for IoT enabling underwater wsns," *IEEE Access*, vol. 5, pp. 10040–10051, 2017.

[5] H. Afrakhte and P. Bayat, "A contingency based energy management strategy for multi-microgrids considering battery energy storage systems and electric vehicles," *J. Energy Storage*, vol. 27, Feb. 2020, Art. no. 101087.

[6] X. Jiang and C. Xiao, "Household energy demand management strategy based on operating power by genetic algorithm," *IEEE Access*, vol. 7, pp. 96414–96423, 2019.

[7] A. S. O. Ogunjuyigbe, T. R. Ayodele, and O. A. Akinola, "Optimal allocation and sizing of PV/wind/split-diesel/battery hybrid energy system for minimizing life cycle cost, carbon emission and dump energy of remote residential building," *Appl. Energy*, vol. 171, pp. 153–171, Jun. 2016.

[8] J.-P. Liu, T.-X. Zhang, J. Zhu, and T.-N. Ma, "Allocation optimization of electric vehicle charging station (EVCS) considering with charging satisfaction and distributed renewables integration," *Energy*, vol. 164, pp. 560–574, Dec. 2018.

[9] M. P. Bonkile and V. Ramadesigan, "Physics-based models in PV-battery hybrid power systems: Thermal management and degradation analysis," *J. Energy Storage*, vol. 31, Oct. 2020, Art. no. 101458.

[10] R. K. Rajkumar, V. K. Ramachandaramurthy, B. L. Yong, and D. B. Chia, "Techno-economical optimization of hybrid pv/wind/battery system using neuro-fuzzy," *Energy*, vol. 36, no. 8, pp. 5148–5153, Aug. 2011.

[11] A. Mosavi, S. N. Qasem, M. Shokri, S. S. Band, and A. Mohammadzadeh, "Fractional-order fuzzy control approach for photovoltaic/battery systems under unknown dynamics, variable irradiation and temperature," *Electronics*, vol. 9, no. 9, p. 1455, Sep. 2020.

[12] P. Raju and S. Vijayan, "Artificial intelligence based battery power management for solar PV and wind hybrid power system," *Int. J. Eng. Res. Gen. Sci.*, vol. 1, no. 2, pp. 37–46, 2013.

[13] M. M. Ismail and A. F. Bendary, "Smart battery controller using ANFIS for three phase grid connected PV array system," *Math. Comput. Simul.*, vol. 167, pp. 104–118, Jan. 2020.

[14] X. Ge, F. W. Ahmed, A. Rezvani, N. Aljojo, S. Samad, and L. K. Foong, "Implementation of a novel hybrid BAT-fuzzy controller based MPPT for grid-connected PV-battery system," *Control Eng. Pract.*, vol. 98, May 2020, Art. no. 104380.

[15] R. Wongsathan and A. Nuangnit, "Optimal hybrid neuro-fuzzy based controller using MOGA for photovoltaic (PV) battery charging system," *Int. J. Control, Autom. Syst.*, vol. 16, no. 6, pp. 3036–3046, Dec. 2018.

[16] A. Ulutas, I. H. Altas, A. Onen, and T. S. Ustun, "Neuro-Fuzzy-Based model predictive energy management for grid connected microgrids," *Electronics*, vol. 9, no. 6, p. 900, May 2020.

[17] Y. Allahvirdizadeh, M. Mohamadian, and M.-R. HaghiFam, "Study of energy control strategies for a standalone PV/FC/UC microgrid in a remote," *Int. J. Renew. Energy Res.*, vol. 7, no. 3, pp. 1495–1508, 2017.

[18] M. Habib, A. A. Ladjici, and A. Harrag, "Microgrid management using hybrid inverter fuzzy-based control," *Neural Comput. Appl.*, vol. 32, pp. 9093–9111, Aug. 2019.

[19] L. W. Chong, Y. W. Wong, R. K. Rajkumar, and D. Isa, "An optimal control strategy for standalone PV system with battery-supercapacitor hybrid energy storage system," *J. Power Sources*, vol. 331, pp. 553–565, Nov. 2016.

[20] T. Wang, M. J. Pérez-Jiménez, J. Wang, J. Ming, Z. Sun, C. Wei, and C. Lu, "Application of neural-like P systems with state values for power coordination of photovoltaic/battery microgrids," *IEEE Access*, vol. 6, pp. 46630–46642, 2018.

[21] H. Harandizadeh, D. J. Armaghani, and M. Khari, "A new development of ANFIS–GMDH optimized by PSO to predict pile bearing capacity based on experimental datasets," *Eng. Comput.*, vol. 9, pp. 177–198, Aug. 21, 2019, doi: 10.1007/s00366-019-00849-3.

[22] M. H. Rezaei, M. Sadeghzadeh, M. A. Nazari, M. H. Ahmadi, and F. R. Astaraei, "Applying GMDH artificial neural network in modeling CO_2 emissions in four nordic countries," *Int. J. Low-Carbon Technol.*, vol. 13, no. 3, pp. 266–271, Sep. 2018.

[23] A. Ardakani and A. Kordnaeij, "Soil compaction parameters prediction using GMDH-type neural network and genetic algorithm," *Eur. J. Environ. Civil Eng.*, vol. 23, no. 4, pp. 449–462, Apr. 2019.

[24] O. Dag and C. Yozgatligil, "GMDH: An R package for short term forecasting via GMDH-type neural network algorithms," *R J.*, vol. 8, no. 1, p. 379, 2016. [Online]. Available: https://journal.r-project.org/archive/2016/RJ-2016-028/RJ-2016-028.pdf

[25] J. Xiao, H. Cao, X. Jiang, X. Gu, and L. Xie, "GMDH-based semi-supervised feature selection for customer classification," *Knowl.-Based Syst.*, vol. 132, pp. 236–248, Sep. 2017.

[26] Z. A. Baig, S. M. Sait, and A. Shaheen, "GMDH-based networks for intelligent intrusion detection," *Eng. Appl. Artif. Intell.*, vol. 26, no. 7, pp. 1731–1740, Aug. 2013.

[27] B. Lin, "Conceptual design and modeling of a fuel cell scooter for urban Asia," *J. Power Sources*, vol. 86, nos. 1–2, pp. 202–213, Mar. 2000.

[28] S. W. Sung, J. Lee, and I.-B. Lee, *Process Identification and PID Control*, vol. 6. Hoboken, NJ, USA: Wiley, 2009.

[29] A. Tofighi and M. Kalantar, "Power management of PV/battery hybrid power source via passivity-based control," *Renew. Energy*, vol. 36, no. 9, pp. 2440–2450, Sep. 2011.

[30] D. E. Kirk, *Optimal Control Theory: An Introduction*. North Chelmsford, MA, USACourier Corporation, 2012.

[31] M. R. Mojallizadeh, M. Badamchizadeh, S. Khanmohammadi, and M. Sabahi, "Designing a new robust sliding mode controller for maximum power point tracking of photovoltaic cells," *Sol. Energy*, vol. 132, pp. 538–546, Jul. 2016.